PROCEEDINGS OF SCIENCE

Radio-Emission from Atmosphere-Skimming Cosmic-Ray Showers in High-Altitude Balloon-Borne experiments

Matias Tueros,[a,*] **Sergio Cabana Freire**[b] **and Jaime Alvarez Muñiz**[b]

[a] *Instituto de Fisica La Plata, CONICET-UNLP, Diagonal 113 entre 63 y 64 , La Plata, Argentina*

[b] *Instituto Galego de Física de Altas Enerxías (IGFAE), Universidade de Santiago de Compostela, 15782 Santiago de Compostela, Spain*

E-mail: tueros@fisica.unlp.edu.ar, sergio.cabana.freire@usc.es, jaime.alvarez@usc.es

Atmosphere-skimming showers are initiated by cosmic rays above the Earth's horizon with incoming directions such that the development of the cascade occurs fully inside the atmosphere. Radio pulses induced by this type of showers have already been observed in balloon-borne experiments such as ANITA, but a characterization of their properties is lacking. The extreme range of densities in which these cascades can develop gives rise to a wide range of shower profiles, with characteristics of the radio emission that can differ significantly from those of regular downward-going showers. To study this type of event, we have used the ZHAireS-RASPASS program, a custom-built modification to the well-known ZHAireS suite capable of simulating atmosphere-skimming showers and calculating their associated radio emission. We have studied the interplay between the magnetic field and atmospheric density profile in the expected signal, focusing on the detection of these events by experiments flying over Antarctica. A new asymmetry in the spatial distribution of the electric field has been identified as a consequence of the very long distances over which the shower particles propagate in the Earth's magnetic field (*the coherence asymmetry*). This asymmetry adds to (but is independent of) the already expected *diffractive asymmetry*, that is a consequence of the propagation of the radio signal through an index of refraction gradient. Finally we briefly discuss the implications of these peculiar characteristics on the expected exposure of balloon-borne experiments, and provide an estimation of the most probable energy for events detected by ANITA IV.

38th International Cosmic Ray Conference (ICRC2023)
26 July - 3 Aug 2023
Nagoya, Japan

ICRC2023
38th International Cosmic Ray Conference
The Astroparticle Physics Conference

*Speaker

PoS(ICRC2023)349

1. Introduction

The study of ultra-high energy cosmic-ray showers has been a cornerstone in the field of astroparticle physics.Traditionally, these showers have been observed and studied as they cascade down through the Earth's atmosphere, producing detectable signals at ground-based observatories. However, the advent of new balloon-borne experimental techniques and instrumentation has unveiled a fascinating new class of cosmic-ray events known as Atmosphere-Skimming showers.

Atmosphere-Skimming (AS) showers are initiated by cosmic rays arriving from above the Earth's horizon with trajectories such that the entire development of the cascade occurs in the atmosphere without the shower core hitting ground (Fig. 1). As the cascade develops, it generates an electromagnetic and hadronic shower front that extends through the atmosphere, spreading out in the direction perpendicular to the local magnetic field due to the Lorentz force. While balloon-borne experiments, such as ANITA [1] flights I to IV, have detected atmosphere-skimming showers[1], a detailed characterization of the emitted radio signals is still lacking. The extreme range of atmospheric densities in which these showers can develop gives rise to a wide variety of shower profiles [2, 3], leading to radio emission characteristics that differ significantly from those of conventional downward-going showers. Understanding and characterizing these differences is crucial to extract the relevant information from the detected radio signals.

To tackle this challenge, we have employed the ZHAireS-RASPASS program [2], a custom-built modification to the ZHAireS/Aires suite [4, 5], specifically designed to simulate AS showers and calculate their associated radio emission. Using ZHAireS-RASPASS, we were able to investigate the interplay between atmospheric density profile, the shower longitudinal development and the invisible energy in the showers in an accompanying contribution [3]. In this contribution, we explore the implications of the unique characteristics of AS showers on their radio emission, and showcase how these can be exploited for the interpretation of data from balloon-borne experiments.

2. Simulation of the radio signal of Atmosphere-Skimming Showers

RASPASS stands for **A**ires **S**pecial **P**rimary for **A**tmospheric **S**kimming **S**howers. It was created in 2011 as an extension module within the Aires shower Monte Carlo simulation program. Its purpose was to simulate special primary particles in response to the detection of the first ANITA above-horizon events. Over time, RASPASS underwent significant evolution and eventually transformed into a standalone version of ZHAireS (Aires with radio emission calculation capabilities). With these advancements, the program now encompasses various modifications to accommodate simulations of diverse shower geometries, including downward-going, upward-going, Earth-skimming, and atmosphere-skimming showers. RASPASS uses physics algorithms identical to the standard Aires and ZHAireS programs. It also adopts the user-friendly input interface from Aires, allowing for seamless integration into existing workflows. One notable enhancement of RASPASS is its ability to simulate showers initiated by multiple primaries, such as the decay products resulting from a tau decay. It also inherits ZHAireS and Aires limitations, the most notable of which is the utilization of a single-layer exponential for the modeling of the index of refraction.

[1] 2, 1, 2 and 2 atmosphere-skimming events were detected in the ANITA I, II, III and IV flights, respectively [6–8]

In this contribution we will focus on the general characteristics of radio emission relevant to balloon-borne detectors. These depend on the frequency band of detection, the atmospheric density profile (and hence the geometry of the shower - see Fig. 1), and on the local magnetic field strength and direction. Throughout this work and for illustrative purposes, we approximate the operation conditions of the ANITA detector by using the average magnetic field and atmospheric profiles of the South Pole. We will be approximating the ANITA detector response to the simulated electric field with a square filter in frequency, and we will use a simple amplitude trigger as done in [9]. The conversion from filtered electric field amplitude $|E_{\text{filter}}(t)|$ to antenna peak voltage V_{peak} is done through a constant that takes into account the properties of the ANITA detector, and reads:

$$V_{\text{peak}} = \max\left(|E_{\text{filter}}(t)|\right) \frac{c}{f_C}\sqrt{\frac{R_L D}{Z_0 4\pi}} \begin{cases} R_L = 50\,\Omega & D = 10\,\text{dBi} \\ Z_0 = 377\,\Omega & f_C = 300\,\text{MHz} \end{cases} . \tag{1}$$

The trigger threshold in ANITA I (III) was set to 141 μV (91 μV). Thus, we consider $V_{\text{peak}} \approx 100\,\mu$V as a typical trigger condition.

3. Lateral distribution of the radio signal

Modeling the earth as a sphere, the geometry of Atmosphere-skimming showers can be characterized solely by the minimum distance between the shower trajectory and the Earth's surface, known as the shower impact parameter b. As depicted in Figure 1, when a balloon detector is being considered, it becomes useful to introduce the zenith angle (θ) and the altitude at which the shower axis reaches the detector location in the z-axis (`RASPASSHeight`).

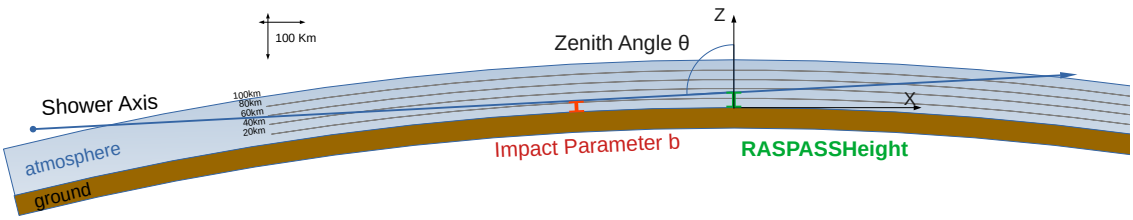

Figure 1: Geometry of an atmosphere-skimming event with impact parameter $b = 24.7$ km, corresponding to a shower with $\theta = 93°$ zenith angle passing at 36 km altitude `RASPASSHeight`. The Earth's curvature is actually shown to scale.

For most values of b the cascade of particles in this type of event unfolds in an extremely rarefied atmosphere compared to regular downward-going events, typically developing in densities smaller than a tenth of the sea level value. This results in a particle cascade that extends along the shower axis for several hundred kilometers, potentially escaping the atmosphere [2, 3]. Moreover, the extended distance inside the low-density atmosphere implies that the Earth's magnetic field strongly influences the motion of the particles, leading to a very significant geomagnetic charge separation. Various effects arise from the charge separation, depending on the orientation of the magnetic field relative to the direction of the shower axis. Analytical calculations and the proposal of several novel detection techniques exploiting this effect where carried out in [10].

At the South Pole, where the magnetic field is nearly perpendicular to the Earth's surface, the shower spreads out strongly in the horizontal direction resulting in a wide spatial distribution in the plane parallel to ground. This has an important effect on the distribution of the radio emission at the detector plane[2].

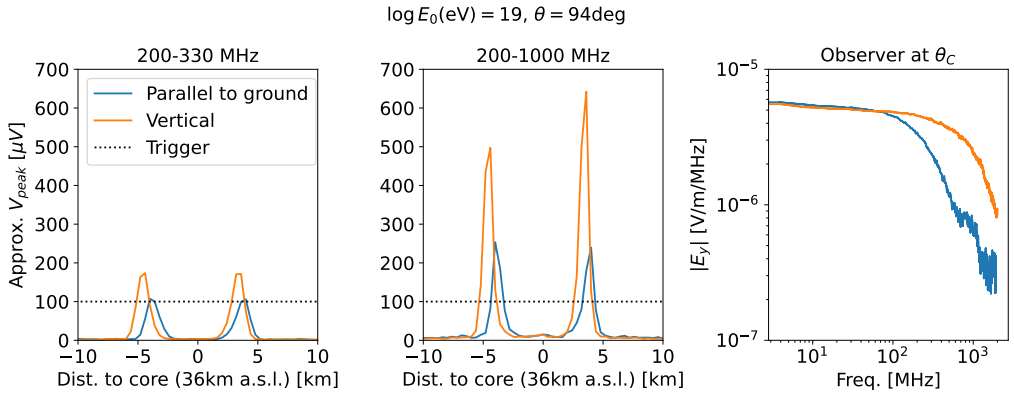

Figure 2: Left and center: Lateral distribution (LDF) of the simulated peak voltage of the electric field obtained with ZHAireS-RASPASS applying Eq.(1) in two different frequency bands, in a proton-induced shower of energy 10^{19} eV and $\theta = 94°$ passing at 36 km a.s.l. The LDF is shown both in the directions parallel to ground and vertical (z-axis in Fig. 1). A typical trigger value of 100 μV is indicated. Right: Frequency spectrum of the simulated electric field for observers at the Cherenkov angle, along the parallel-to-ground (blue) and vertical (orange) direction. The spectra correspond to the signals observed at the peaks to the "right" of the radio LDF shown in the central panel.

The simulated lateral distribution (LDF) of the amplitude of the radio signal registered in the plane of the detector, both in the directions parallel to ground (y) and vertical (z), is shown in Fig. 2 for a typical AS event and for two frequency bands. The LDF is characterized by two distinct peaks as in regular down-going events, approximately corresponding to the positions where the shower maximum is observed under the Cherenkov angle, and resulting in a maximally coherent signal. However, two notable asymmetries are observed in AS events. The first arises in the vertical direction, where the LDF is slightly displaced from the origin towards lower altitudes (negative values of distance to the core in Fig. 2). Since AS showers traverse the atmosphere in a nearly horizontal direction, the optical path between the source and an observer situated above or below the shower axis differs significantly due to the different gradient of index of refraction. As a result, the *effective* Cherenkov angle is decreased or increased, leading to a displacement effect [11]. In contrast, this displacement is not present in the horizontal direction, as the optical paths with respect to the shower axis are very similar in the plane parallel to ground. This magnetically-induced *coherence asymmetry* is observed in the peak voltages, highlighting the impact of geomagnetic deflection on these events. Due to the low densities and the large distances over which AS showers develop, the geomagnetic field deflects the particles to the point that the shower front is strongly spread out in the direction of the Lorentz force. Consequently, time delays between different parts of the shower front are increased when the emission is observed along the direction of deflection

[2]This is the plane perpendicular to the projection of the shower axis on ground at the position where the shower axis crosses the z-axis (the position of an imaginary detector)

(the horizontal direction in Fig. 2). This leads to a reduction in the frequency at which the emission begins to add incoherently and a decrease in the high-frequency content of the signal, as it can be seen in the frequency spectrum of the signal shown in Fig. 2, right. The amplitude asymmetry between the LDFs along the direction parallel and perpendicular to the Lorentz force becomes more pronounced when the high-frequency content is included in the signal after filtering (Fig. 2 center). As shown below, this amplitude asymmetry can restrict the detectable geometries depending on the primary energy and frequency range of detection, as shown in Fig. 2 left, where only the peak voltage induced in the vertical direction is above the trigger threshold.

In view of the LDFs shown in Fig. 2, it becomes clear that the shape of the region on the detector plane where the radio signal is strong enough to produce a trigger (radio footprint) will be very dependent on the zenith angle of the shower. Small changes in θ translate into large variations in the distance between $X_{\max}$ and the plane of the detector [3]. Furthermore, the emission takes place over significantly different density profiles, changing the opening angle of the Cherenkov cone. These two effects influence the size of the radio footprint at the detector plane, also enhancing or reducing the aforementioned asymmetries. To give an idea of the scale of these changes, in Fig. 3 we present the approximate radio footprint for an experiment like ANITA. The shape of the region is obtained from the LDF, using the points where the signal falls below a given threshold to fit the elliptic regions shown in red.

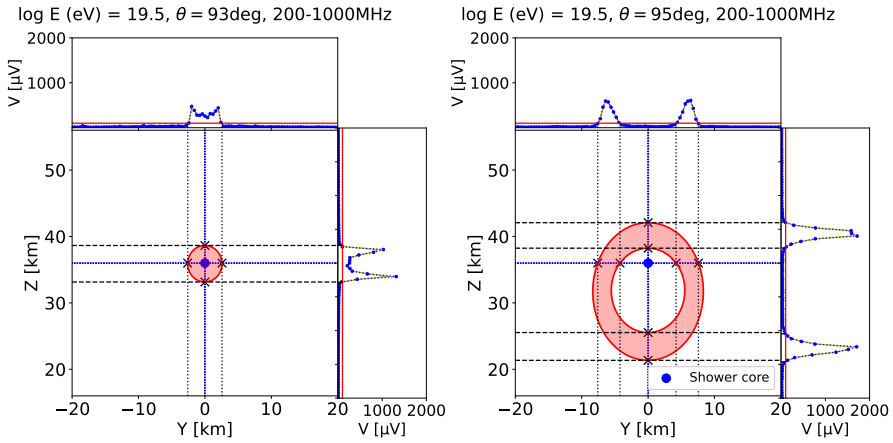

Figure 3: Shape of the radio footprint in the detector plane (shaded red area), fitted using the vertical (along z) and parallel-to-ground signal (along y) LDFs (see Fig. 2 for an example), for two proton-induced showers with energy $10^{19.5}$ eV and $\theta = 93°$ and 95°, passing at 36 km a.s.l. (Fig. 1). The blue dot indicates the position of the shower axis in the detector plane. The trigger threshold was set to $V_{\text{peak}} = 100\,\mu$V.

For the shower with $\theta = 93°$ in Fig. 3, that develops at a higher altitude in the atmosphere than the one with $\theta = 95°$, the position of $X_{\max}$ is closer to the detector and the shower develops in a less dense atmosphere. As a consequence, the Cherenkov angle is smaller and the Cherenkov cone is less open in the detector plane, producing a significantly smaller footprint. Depending on the trigger threshold and the shower θ, the peaks in the LDF can be unresolved, and in that case the active radio footprint of the shower is a filled circle around shower core. The shower with $\theta = 95°$ in Fig. 3 develops at a lower altitude, and the position of $X_{\max}$ is further away from the detector and

in a denser region of the atmosphere, having an increased Cherenkov opening angle and cone size at the detector when compared with the shower at $\theta = 93°$. As a consequence, at high enough energy, the trigger area is a ring-like elliptical region as shown in the right panel of Fig. 3. For $\theta = 95°$, the displacement of the footprint in the vertical direction due to the gradient of refractive index is apparent, with the footprint greatly displaced towards lower altitudes. For constant θ, changing the value of the `RASPASSHeight` of the event (the altitude of the shower core on the detector plane) affects the shape and size of the active area in a similar way.

These features of the radio LDF of AS showers, together with their dependence on the nature of the primary particle, energies, zenith angle, and detector altitude, will produce non-trivial changes in the shape of the detectable region around the shower core, that cannot be in general described in terms of simple geometric shapes. Understanding the exposure of a detector to AS events will require a detailed and comprehensive simulation study, that would need also to take into account the evolution with time of detector altitude, atmospheric conditions, magnetic field orientation, etc.

4. Effective trigger area and exposure of balloon-borne experiments.

The effective area for detection at a given primary energy E_0 and direction $A_{\rm eff}(E_0, \theta, \phi, h_{\rm det})$ for a balloon-borne experiment located at a fixed detector height $h_{\rm det}$ can be estimated with simulations varying uniformly the position of the shower core around the detector for fixed values of (E_0, θ, ϕ). In that case, the effective area can be obtained as:

$$A_{\rm eff}(E_0, \theta, \phi, h_{\rm det}) \sim A_{\rm sample} \frac{N_{\rm trig}}{N_{\rm tot}} \cos\left(\theta - \frac{\pi}{2}\right) , \tag{2}$$

where $N_{\rm trig}/N_{\rm tot}$ is the ratio between the number of core positions that produce a trigger in the detector and the total number of sampled positions, and $A_{\rm sample}$ is the sampled area in the detector plane. The last term accounts for the projection of the area in the plane of the detector along the shower direction.

In particular, we simulated a batch of p and Fe-induced showers with different E_0 and impact parameter b, fixing the direction (θ, ϕ) and the detector height to the the values corresponding to the two above-horizon events seen in the ANITA-IV flight [8], for which no energy estimation has been published yet. The magnetic field and atmospheric density was set according to the date of the events using the IGRF model [12]. A refractivity profile compatible with the density profile in the range of altitudes where these showers develop was obtained through a fit of the values computed with the GDAS database [13]. The effective area for one of the two atmosphere-skimming events detected with ANITA-IV is shown in Fig. 4, for p and Fe primaries. As expected, the detection area grows with E_0. It also becomes clear that showers passing above or below the detector produce stronger signals at the detector than showers passing to the side, which is a consequence of the *coherence asymmetry* discussed in Sec. 3. This effect is especially important at the lowest energies shown, where only showers passing above/below the detector can produce a trigger. The effective area is asymmetric around the detector and displaced in the upward direction. This is a consequence of the displacement of the radio footprint due to the gradient of refractive index shown in Fig. 3. Also, as showers passing below the detector go through more dense regions, the projection of the Cherenkov cone at the detector plane is larger, producing the widening of the effective area

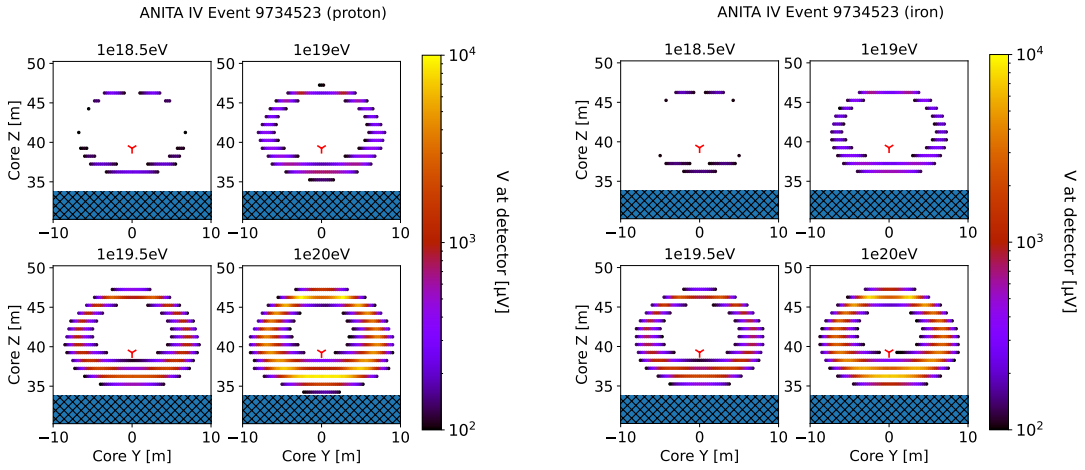

Figure 4: Effective area around the position of the detector for one of the two Atmosphere-Skimming events (ID: 9734523) detected by ANITA IV [8], for proton and iron primaries of different energies. The colored areas represent the positions where shower cores can produce a trigger at the position of the detector (red symbol). The color scale indicates the peak voltage induced by the shower. The *coherence asymmetry* and the refractive index displacement determine the shape of the area (see text for explanation). The striped region at the bottom of each plot represent geometries with a negative impact parameter (showers hitting ground and not visible) at the incoming direction reported in for this specific event.

below the detector. Finally, the effective area for Fe showers is slightly smaller than that of proton showers. This effect can be tracked to the differences in distance between $X_{\rm max}$ and detector and in the invisible energy that arise in AS showers depending on the primary particle, as discussed in [3].

The effective area, can be multiplied by the cosmic-ray flux above 10^{17} eV as measured by the Pierre Auger Observatory [14] to estimate the most probable energy of the AS events detected by ANITA IV. This is shown in Fig. 4. Due to the similar zenith angle ($\theta_{9734523} = 95,64°$; $\theta_{51293223} = 95,38°$) and payload height ($H_{9734523} = 39,25\,$km; $H_{51293223} = 37,53\,$km) in both events, the results are rather similar. The growth of the effective area with the primary energy is not enough to compensate for the steep cosmic-ray spectrum above $\sim 10^{18.5}$ eV placing an approximate energy threshold for the detection of a cosmic ray with these incoming directions between 1 and 3 EeV. Also, it can be seen that the most probable energy is close to the threshold value, slightly higher when considering Fe as primary particle. In any case, the most likely energies of the two ANITA IV events should be taken as simple estimates, always keeping in mind that these results lack the detailed modeling of the ANITA response.

5. Conclusions

The radio emission associated to atmosphere-skimming air showers features unique characteristics of relevance when interpreting real data or estimating the aperture of different experiments. The lateral distribution function of the radio signal in the detector plane exhibits asymmetries that strongly depend on shower geometry and altitude of the detector and that strongly influence the effective area of balloon-borne experiments to this type of showers. In particular, we have discovered

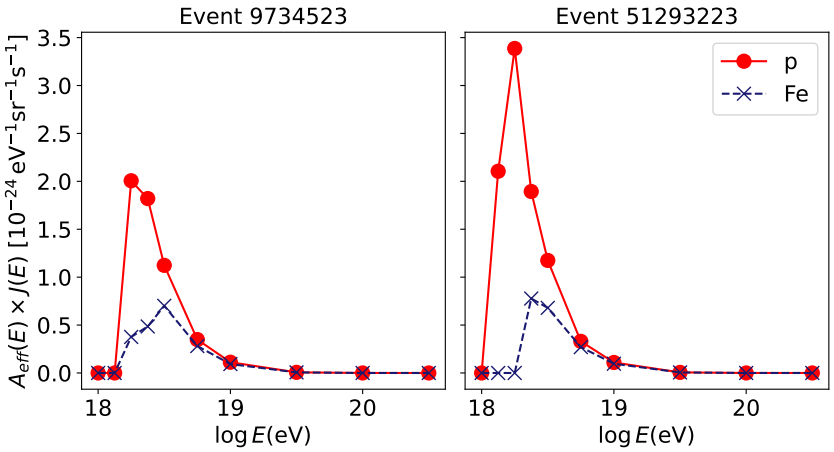

Figure 5: Effective area for cosmic ray detection at the reported incoming direction of the two above-horizon events in ANITA IV [8]. The effective areas of the two Atmosphere-Skimming events detected by ANITA IV (see an example in Fig. 4) multiplied by the cosmic-ray flux as measured by Auger, giving an estimate of the most likely energy of the two events depending on the primary particle (p or Fe) assumed.

evidence of a new source of asymmetry in the radio footprint (the *coherence asymmetry*), consisting in a higher amplitude and frequency content for positions above and below the plane containing the Lorentz force and the primary direction of motion. This is induced by the extreme spread of the shower front along this plane, a consequence of the development of the cascade over very long distances in the Earth's magnetic field. Our results demonstrate the power of the ZHAireS-RASPASS simulation to study the physics of Atmosphere-Skimming events.

Acknowledgments: This work is funded by Xunta de Galicia (CIGUS Network of Research Centers & Consolidación ED431C-2021/22 and ED431F-2022/15); MCIN/AEI PID2019-105544GB-I00 - Spain; European Union ERDF.

References

[1] R. Prechelt *et al.* Phys. Rev. D **105**, 042001 (2022) and references therein.
[2] M. Tueros. PoS(ARENA2022)056.
[3] M.Tueros, S. Cabana Freire, J. Alvarez-Muñiz, PoS(ICRC2023)348.
[4] S. J. Sciutto [arXiv:astro-ph/9911331]; http://aires.fisica.unlp.edu.ar
[5] J. Alvarez-Muñiz *et al.* Phys. Rev. D **86**, 123007 (2012)
[6] P. W. Gorham *et al.* Phys. Rev. Let., **117**, 071101 (2016).
[7] P. W. Gorham *et al.* Phys. Rev. Lett., **121**, 161102 (2018).
[8] P. W. Gorham *et al.* Phys. Rev. Lett. **126**, 071103 (2021).
[9] A. Romero-Wolf *et al.*, Phys. Rev. D, **99**, 063011 (2019).
[10] D. Fargion *et al.* PoS(ICRC2021)1208 and references therein.
[11] F. Schlüter *et al.* Eur. Phys. J. C **80**, 643 (2020).
[12] P. Alken et al. , Earth Planets Space **73**, 49 (2021).
[13] P. Mitra et al., Astrop. Phys. **123**, 102470 (2020)
[14] Pierre Auger Collaboration. Eur. Phys. J. C **81**, 966 (2021).